

The magnetoelectric properties of A- or B-site-doped PbVO₃ films: A first-principles study*

Chen Xing-Yuan(陈星源), Chen Li-Juan(陈丽娟), and Zhao Yu-Jun(赵宇军)[†]

Department of Physics and State Key Laboratory of Luminescent Materials and Devices, South China University of Technology, Guangzhou 510640, China

(Received 21 October 2012; revised manuscript received 26 February 2013)

We employ first-principles calculations to study the magnetic and ferroelectric properties of PbVO₃ with A ($X_A = \text{Ca, Sr, Bi, Ba, and La}$) or B ($X_B = \text{Ti, Cr, Mn, Fe, Co, Ni, and Cu}$) site dopants, with the aim of ascertaining a large ferroelectric polarization and a long magnetic order, or even a macro ferri/ferromagnetism, which is critical to their potential applications in magnetoelectronic devices. It is found that Pb₇X_AV₈O₂₄ ($X_A = \text{Ca, Sr, and Ba,}$) are inclined to maintain the spin glass and large ferroelectric polarization. The degenerated G- and C-antiferromagnetic (AFM) couplings in the ideal PbVO₃ are broken up, accompanied by the loss of ferroelectric properties, when La or Bi is doped at the A site. In contrast, the above-mentioned 3d transition elements doped at the B site of PbVO₃ could induce remnant magnetic moments and preserve the large ferroelectric polarization, except for Ni and Cu. The Fe or Cr at the B site clearly remove the degenerated G- and C-AFM coupling, but the nonmagnetic Ti cannot do so. For the Mn, Co, Ni, or Cu doped at the B sites, even the two-dimensional AFM ordering in PbVO₃ is destabilized. The various doping effects are further discussed with inner strain and charge transfer.

Keywords: multiferroic, magnetism, ferroelectric, doping

PACS: 77.55.Nv, 75.85.+t, 74.62.Dh

DOI: 10.1088/1674-1056/22/8/087703

1. Introduction

Multiferroic materials, holding two or more ferroelectric, ferroelastic, and (anti)ferromagnetic orderings, have demonstrated rich physics connotations and great potential applications.^[1] Single-phase multiferroic materials mainly focus on ABO₃ perovskite oxides.^[2,3] PbVO₃ as a candidate of multiferroic materials has attracted much attention in the past decade.^[4–9] Bulk PbVO₃ is known to be a PbTiO₃-type structure with a large tetragonal distortion ($c/a = 1.22$) under high temperature (HT) and high pressure (HP) conditions.^[8] Its ferroelectric polarization has been predicted to be as large as 152 $\mu\text{C}/\text{cm}^2$ by first-principles calculations.^[10] The P - E hysteresis of polarization is not observed in PbVO₃ due to its low resistivity in ferroelectric measures.^[8]

Interestingly, the PbVO₃ films that were grown on the LaAlO₃ (001) substrate by pulsed laser deposition^[7] can be stabilized in an even greater tetragonally distorted perovskite structure ($c/a = 1.32$) and exhibit piezoelectricity at room temperature.^[7,11] Both theoretical and experimental studies have shown that V ions in bulk PbVO₃ are arranged in two-dimensional antiferromagnetic (AFM) ordering.^[6,8,11–13] PbVO₃ films also display a two-dimensional AFM ordering in the a - b plane.^[12] It was predicted that PbVO₃ possesses a long ordering of C-type antiferromagnetism and a weak magnetoelectric coupling under 120 K by density functional theory calculations.^[6] G-type antiferromagnetism was also predicted

to be the ground state for PbVO₃ grown on a wide range of substrates.^[14,15] However, a long magnetic order is difficult to realize in PbVO₃ samples as it is often coupled to a spin glass phase.^[4,11] This is mainly ascribed to an obvious competition between G- and C-type AFM ordering in PbVO₃ with a weak magnetic coupling along the z direction.^[6] Of note, C- and G-type AFMs have the same magnetic arrangement in the a - b plane, while they couple ferromagnetically and antiferromagnetically along the z direction. Recently, Solovyev^[16] analyzed the possible magnetic structure of PbVO₃ using a low-energy electronic model and argued that PbVO₃ should form a long periodic spin-spiral state with a period of about 100 unit cells, resulting solely from the competition between the isotropic exchange and Dzyaloshinskii–Moriya interactions in the noncentrosymmetric crystal structure. Similar to the case of PbVO₃, the verified magnetic structure of BiFeO₃ shows a long-wavelength spiral structure with 620 Å in the bulk deviation from the ideal G-type ordering and a slight canting of the magnetic moments in the thin films.^[17,18] Though the magneto-electrical coupling of PbVO₃, as a proper multiferroic material, is expected to be weak, a long magnetic ordering in PbVO₃ could bring richer physics connotations into the systems of interest.

Meanwhile, the multiferroic properties of ABO₃ perovskite oxides can often be improved by introducing magnetic dopants as long as their ferroelectric properties can be main-

*Project supported by the National Natural Science Foundation of China (Grant No. 11174082) and the Education Foundation of Science and Technology Innovation of the Ministry of Education, China (Grant No. 708070).

[†]Corresponding author. E-mail: zhaoyj@scut.edu.cn

tained. ABO_3 perovskite oxides can be doped at either the A or B sites, often leading to different physical properties. As a typical multiferroic material, $BiFeO_3$ has been studied with both A- and B-site dopings to improve its multiferroic property.^[19–24] It has been reported that the original spiral G-AFM spin configuration of $BiFeO_3$ can be suppressed effectively by A-site doping with ions of larger ionic radii.^[22,25] Furthermore, A-site doping in $BiFeO_3$ with La and Ba was reported to enhance the magnetization and showed some remnant magnetic moments.^[26,27] B-site doped Bi_2FeCrO_6 was predicted to be a ferrimagnetic and ferroelectric material with a magnetic moment of $2 \mu_B/f.u$ by theoretical calculations,^[20] and this was later confirmed experimentally.^[21] Cr- or Fe-doped $BiCoO_3$ was also predicted to be ferrimagnetic, while its excellent ferroelectric property is maintained.^[28] Here, we attempt to stabilize a long magnetic order, or even net magnetic moments, and large ferroelectric polarization in $PbVO_3$ by A- or B-site doping. It is found that the spin glass and large ferroelectric polarization can be maintained by doping Ca, Sr, and Ba at the A site, and the spin glass and ferroelectric properties are absent when La or Bi is doped at the A-site. The 3d transition element doping at the B site of $PbVO_3$ can bring a remnant magnetic moment and preserve the large ferroelectric polarization, except for Ni and Cu.

2. Computational method

All the calculations are carried out by a planewave method with interactions between the valence electrons and ions represented by the projector augmented wave (PAW) pseudo-potentials, as implemented in the Vienna *ab-initio* simulation package (VASP).^[29,30] The generalized gradient approximation (GGA) of the PW91 functional for the exchange and correlation potential is employed.^[31] The GGA + U method is also used for the strongly-correlated nature of the 3d transition metal ions to obtain the accurate electronic structure. Here, U represents the on-site repulsion energy term originating from the Hubbard model for strong correlated systems.^[32] A typical value of $U_{eff} = 4$ eV, as in earlier studies,^[33,34] is applied to the TM d states in our GGA + U calculations to check the effect of the Hubbard U correction. The energy cutoff is set to be 500 eV and a $6 \times 6 \times 6$ Monkhorst–Pack grid is adopted in the calculations. Since the energy difference between the various magnetic orderings is rather small, we carefully check the convergence with respect to the cutoff energy and k mesh. It is found that the changes in the calculated total energy difference between the C- and G-AFM configurations are within 0.1 meV/formula as the energy cutoff and Monkhorst–Pack grid increase up to 700 eV and $8 \times 8 \times 8$ mesh, respectively. The ionic positions are fully relaxed until the Hellman–Feynman forces are less than 0.01 eV/Å in the calculations.

As shown in Fig. 1, a $2 \times 2 \times 2$ supercell of $PbVO_3$ containing 40 atoms is adopted to simulate both the A- and B-site doping.

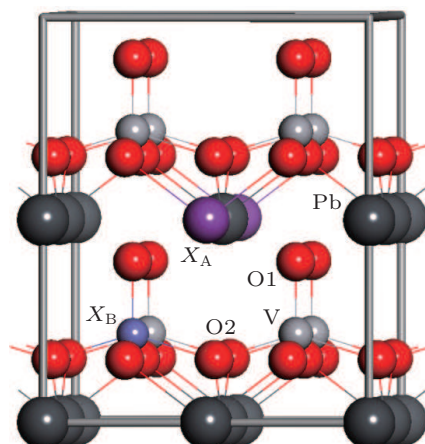


Fig. 1. (color online) A $2 \times 2 \times 2$ $PbVO_3$ superlattice for A- or B-site doping ($X_A = Ca, Sr, Bi, Ba,$ and $La,$ and $X_B = Ti, Cr, Mn, Fe, Co, Ni,$ and Cu). The Pb, V, and O ions are denoted by the dark grey, light grey, and red balls, respectively, with two nonequivalent oxygen ions marked as O1 and O2.

X_A ($X_A = Ca, Sr, Bi, Ba,$ and La) and X_B ($X_B = Ti, Cr, Mn, Fe, Co, Ni,$ and Cu) are denoted as the A- and B-site dopants, respectively. $PbVO_3$ contains nonequivalent oxygen ions: O1 ions are located at the top of the pyramid structures along the z direction and O2 ions are stacked in the a – b plane equivalently. To reduce the computational effort, we assume here that the dopants are uniformly distributed in the lattice, which could be potentially achieved by the state-of-art molecular beam epitaxial techniques.

3. The structure and magnetoelectric properties of $PbVO_3$ film without doping

The C- and G-AFM configurations are almost degenerated in tetragonal $PbVO_3$, which has a weak magnetic coupling along the c direction^[6] between the V^{4+} ions with local magnetic moments of nearly $1 \mu_B$ per ion. We simulate $PbVO_3$ films deposited on $LaAlO_3$ (001) substrates by fixing the (a, b) plane lattice of $PbVO_3$ at that of the $LaAlO_3$ lattice parameter (3.79 Å), with the c lattice vector optimized accordingly. Our calculated results indicate that the $PbVO_3$ film of both the C- and G-AFM configurations is tetragonally distorted with the optimized c at 4.94 Å. These calculated lattice parameters are in good agreement with the experimental values.^[7] The 3d electrons of V^{4+} mainly occupy the d_{xy} level and exhibit magnetic moments $0.95 \mu_B/ion$ and $1.10 \mu_B/ion$ according to our GGA and GGA + U calculations, respectively, which is largely in line with the earlier calculations.^[6,12] We find that the degenerations of the C- and G-AFM configurations are remarkably hard to remove, even with lattice strain, as the energy difference is less than 1 meV/f.u when lattice c changes from 4.94 Å (at optimal) to 4.62 Å (cf. Fig. 2).

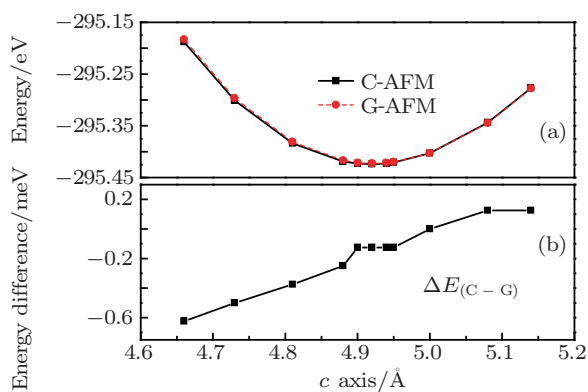


Fig. 2. (color online) (a) The total energies of PbVO_3 with the C- and G-AFM configurations, and (b) the energy difference between them (in meV/f.u.), as a function of lattice constant c when lattice constants a and b are fixed to be those of the LaAlO_3 substrate (3.79 Å).

In fact, PbVO_3 films were widely simulated in a wide range of substrates by density functional calculations, with the aim of decoupling the G- and C-AFM configurations by introducing misfit strains.^[14] However, the energy difference between them is no more than 0.1 meV/f.u.~0.4 meV/f.u., when the misfit substrate size is about 1.6%~4.2%.^[14] This indicates that the lattice strain induced by various substrates can-

not remove the degenerations of the C- and G-AFM configurations well, and thus we cannot introduce a long magnetic order into PbVO_3 . Our calculated ferroelectric polarizations of PbVO_3 film (3.79 Å) and bulk (3.89 Å) are 156.4 $\mu\text{C}/\text{cm}^2$ and 148.7 $\mu\text{C}/\text{cm}^2$, respectively, by the modern polarization theory of the Berry phase method,^[35] which are in agreement with the earlier results.^[10] Subsequently, we mainly discuss the magnetoelectric properties of A- or B-site doping PbVO_3 film with its (a, b) plane lattices fixed to be those of LaAlO_3 (001), which is often reported to be the substrate of PbVO_3 film experimentally.

4. PbVO_3 film with A-site doping

In this section, we attempt to discuss the decoupling of C- and G-AFM configuration and ferroelectric polarization in PbVO_3 by A-site doping. The elements Ca, Sr, Ba, Bi, Pb, La, etc. are typical elements for the A-site dopants in ABO_3 perovskite oxides. Here, $\text{Pb}_7\text{X}_{\text{A}1}\text{V}_8\text{O}_{24}$ ($\text{X}_\text{A} = \text{Ca, Sr, Bi, Ba, and La}$) are studied on the assumption that the dopants are uniformly distributed. The calculated energies of the corresponding C- and G-AFM configurations are listed in Table 1.

Table 1. The energy differences of $\text{Pb}_7\text{X}_{\text{A}1}\text{V}_8\text{O}_{24}$ ($\text{X}_\text{A} = \text{Ca, Sr, and Ba}$) between their G- and C-AFM configurations with GGA and GGA + U , the calculated polarization values along the (001) direction, and the displacements of the impurities with respect to the corresponding lattice site in pure PbVO_3 . The positive and negative values refer to shifting up and down, respectively (cf. Fig. 1).

X_A	Ca	Sr	Ba	Bi	La
$[E(\text{G})-E(\text{C})]/(\text{meV}/\text{X}_\text{A})$ GGA	6	9	7	4	10
$[E(\text{G})-E(\text{C})]/(\text{meV}/\text{X}_\text{A})$ GGA + U	3	2	2	28	16
Band gap/eV	1.72	1.66	1.63	0	0
$P_s/(\mu\text{C}/\text{cm}^2)$	142.6	154.8	152.8	-	-
Displacement/Å	C-AFM	0.140	0.347	-0.108	0.094
	G-AFM	-0.057	0.145	0.349	-0.106

Unlike the degenerated energies of the C- and G-AFM configurations in the pure PbVO_3 , $\text{Pb}_7\text{X}_{\text{A}1}\text{V}_8\text{O}_{24}$ ($\text{X}_\text{A} = \text{Ca, Sr, Bi, Ba, and La}$) favors the C-AFM configuration by 4 meV~10 meV without considering the Hubbard U correction, though the energy difference is still small. When the Hubbard U correction is applied, however, the energy differences between $\text{Pb}_7\text{X}_{\text{A}1}\text{BiV}_8\text{O}_{24}$ and $\text{Pb}_7\text{X}_{\text{A}1}\text{LaV}_8\text{O}_{24}$ are 28 meV and 16 meV per Bi/La, showing a much greater stability of the C-AFM configuration. As listed in Table 1, the band gaps of $\text{Pb}_7\text{X}_{\text{A}1}\text{V}_8\text{O}_{24}$ ($\text{X}_\text{A} = \text{Ca, Sr, Bi, Ba, and La}$) calculated by the GGA + U method indicate that PbVO_3 doped by Bi or La shows no band gap and becomes metallic, which may cause the stability of the C-AFM configuration. This indicates that the degenerations of the G- and C-AFM configurations in the PbVO_3 system can be removed by substituting for A-site dopants.

Typically, in the A site doped by the BiFeO_3 system, it

is found from $\text{Bi}_x\text{A}_{1-x}\text{FeO}_3$ ($\text{A} = \text{Ca, Sr, Pb, and Ba}$) that the spiral spin configuration of AFM BiFeO_3 may be suppressed effectively and that spontaneous polarization is permitted with the substitution of ions of larger ionic radius into the A site to introduce inner physical strain or a mismatched valence state.^[22,25] The Pb ion of PbVO_3 was demonstrated to be in the 2+ valence state experimentally.^[8] Ca^{2+} , Sr^{2+} , Ba^{2+} are also common A-site elements in the perovskite materials, while Bi and La ions are usually active in the 3+ valence state. The ionic radii of Ca^{2+} , Sr^{2+} , Ba^{2+} , Bi^{3+} , La^{3+} , and Pb^{2+} are 0.99, 1.13, 1.35, 0.96, 1.06, 1.20 Å, respectively.^[36] The mismatched ionic radii can cause strains in the relaxed structures of Ca-, Sr-, Ba-, Bi-, and La-doped PbVO_3 . The relative displacements between A-site impurity (Ca, Sr, and Ba) and the corresponding Pb site in pure PbVO_3 are also listed in Table 1. The ferroelectric polarizations along the (001) direction are 152.8 $\mu\text{C}/\text{cm}^2$ and 154.8 $\mu\text{C}/\text{cm}^2$ when doped with Sr and Ba,

respectively, while the ferroelectric polarization decreases to $142.6 \mu\text{C}/\text{cm}^2$ when doped with Ca as relatively smaller displacements are involved with ions of smaller ionic radii. By contrast, $\text{Pb}_7\text{X}_{\text{A}1}\text{V}_8\text{O}_{24}$ ($X_{\text{A}} = \text{Bi}, \text{La}$) have become metallic (Fig. 3) and show no ferroelectric polarization even when the Hubbard U value increases to 10 eV.

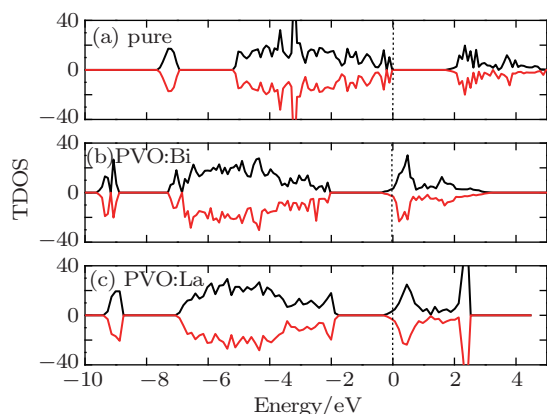


Fig. 3. (color online) The total densities of states of (a) pure, (b) Bi-doped PbVO_3 , and (c) La-doped PbVO_3 corresponding to GGA + U calculations, where the Fermi energy is set to be 0 and the spin-up and spin-down plots are denoted by positive and negative values, respectively.

Here we demonstrate that the A-site substitution can be an effective way to break out the competition between the C- and G-AFM configurations, and potentially form a long-order C-AFM configuration instead of the spin glass mixed with C- and G-AFM orderings. However, the $\text{Pb}_7\text{X}_{\text{A}1}\text{V}_8\text{O}_{24}$ ($X_{\text{A}} = \text{Ca}, \text{Sr}, \text{Bi}, \text{Ba}, \text{and La}$) still hold no remnant magnetic moment or lead to no ferroelectric polarization. In the following section, we discuss the possibility of improving the magnetoelectric property of PbVO_3 by doping 3d transition metals at the B site.

5. PbVO_3 film with B-site doping

It was reported that ferrimagnetism could be achieved in ABO_3 perovskite oxide multiferroic material by doping transition metal at the B-site. Typically, $\text{Bi}_2\text{FeCrO}_6$, the B-site Cr-ion-doped BiFeO_3 , was demonstrated to have ferrimagnetism and showed strong ferroelectric polarization.^[21] Here, $\text{Pb}_8\text{V}_7\text{X}_{\text{B}}\text{O}_{24}$ ($X_{\text{B}} = \text{Ti}, \text{Cr}, \text{Mn}, \text{Fe}, \text{Co}, \text{Ni}, \text{and Cu}$) are used to simulate the B-site doping effect. All of the B-sites doping $\text{Pb}_8\text{V}_7\text{X}_{\text{B}}\text{O}_{24}$ are relaxed from their original C- and G-AFM configurations. The GGA and GGA + U calculated energy differences between the C- and G-AFM configurations, as well as the local magnetic moments at the dopants and the total magnetic moments, are displayed in Fig. 4.

The DFT + U method usually gives more accurate electronic structures for strongly correlated material d electron systems with narrow bands by adding a Hubbard Coulomb

interaction.^[37] It is clear that the GGA + U results show significant energy separations between the C- and G-AFM configurations for $\text{Pb}_8\text{V}_7\text{X}_{\text{B}}\text{O}_{24}$ with $X_{\text{B}} = \text{Cr}, \text{Fe}, \text{Co}, \text{Ni}, \text{and Cu}$, while the GGA results generally gave negligible energy differences. When $X_{\text{B}} = \text{Ti}$, the degenerations of the C- and G-AFM configurations are hard to remove in $\text{Pb}_8\text{V}_7\text{X}_{\text{B}}\text{O}_{24}$, since Ti ions (d^0) are non-magnetic and cannot break the weak magnetic interaction along the c direction. However, the C-AFM configuration takes advantage in Fe-doped PbVO_3 .

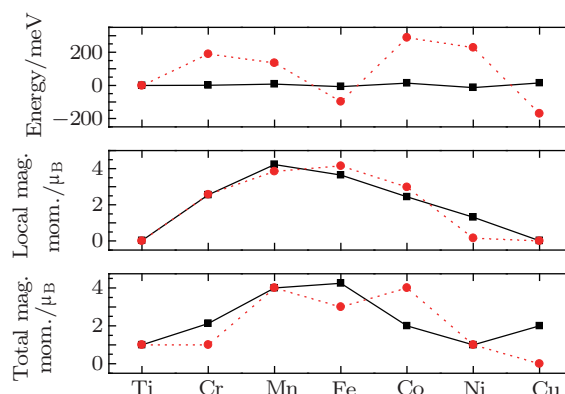


Fig. 4. (color online) (a) The energy difference between the G- and C-AFM configurations, (b) the local magnetic moments of the B-site dopants, and (c) the total magnetic moments of $\text{Pb}_8\text{V}_7\text{X}_{\text{B}}\text{O}_{24}$ ($X_{\text{B}} = \text{Ti}, \text{Cr}, \text{Mn}, \text{Fe}, \text{Co}, \text{Ni}, \text{and Cu}$) calculated by GGA (circular dots) and GGA + U (rectangular dots).

The local magnetic moment of the V ions near the Fe ion is lowered down to about $0.5 \mu_{\text{B}}$, while that of the Fe ion is about $3.6 \mu_{\text{B}}$ in both the GGA + U and GGA calculations. The O2 ion ($0.25 \mu_{\text{B}}$) within a sphere of radius of 0.820 \AA near the Fe ion gains more spin charges than the other O2 ion ($0 \mu_{\text{B}}$), while the V ion near the Fe ion gains less spin charges than the other V ions through the Fe–O2–V interaction (cf. Fig. 5(b)).

The Fe ion with a large magnetic moment could provide some remnant magnetic moments at the O ions and degrade the magnetic moment of the V ions by Fe–O ($0.25 \mu_{\text{B}}$)–V superexchange interaction.^[38] Therefore, the spin glass of PbVO_3 can be dissipated to pose a long magnetic order by Fe doping. In fact, tetragonal ceramic $\text{PbV}_{1/2}\text{Fe}_{1/2}\text{O}_3$ was successfully synthesized under 7 GPa experimentally, and found to have no spin glass phenomenon.^[39] The Cr^{4+} ion (d^2) has a low 3d electronic configuration with a local magnetic moment of about $2.5\text{-}\mu_{\text{B}}$, and takes advantage by G-AFM configuration, while the local magnetic moment of the V ions near the Cr ion is lowered to about $0.8 \mu_{\text{B}}$ and the O ions gain no local magnetic moment. Of note, the V ions along the a - b plane in $\text{Pb}_8\text{V}_7\text{X}_{\text{B}}\text{O}_{24}$ ($X_{\text{B}} = \text{Ti}, \text{Cr}, \text{and Fe}$) still approximately keep the two-dimensional AFM coupling.

By contrast, $\text{Pb}_8\text{V}_7\text{X}_{\text{B}}\text{O}_{24}$ ($X_{\text{B}} = \text{Mn}, \text{Co}, \text{Ni}, \text{and Cu}$) destroy the original two-dimensional AFM ordering of PbVO_3 , leading to a new magnetic ground state locally. Some of the V ions along the a - b plane (as shown in Fig. 5(c) for $\text{PbVO}_3\text{:Co}$)

experience spontaneous spin flips to a new magnetic ground state. It was reported that V^{4+} ions in $PbVO_3$ reveal significant magnetic frustration of the square lattice, which prevents $PbVO_3$ from realizing long-range spin ordering down to 1.8 K.^[12] This indicates that the V^{4+} (d^1) magnetic ions of the square structure in the tetragonal lattice (Fig. 1) play an important role in keeping V^{4+} with two-dimensional AFM

coupling.^[12] The original V-V two-dimensional AFM ordering in the a - b plane is replaced, and this is possibly ascribed to the fact that the B-site ions (Mn, Co, Ni, and Cu) induce a large structural mismatch in $PbVO_3$. While the bond lengths of V-O1 and V-O2 are 1.68 Å and 1.99 Å (Fig. 6) respectively, the length of the B-O1 ($X_B = Mn, Co, Ni$ and Cu) and B-O2 bonds are accordingly more than 1.9 Å and 2.1 Å.

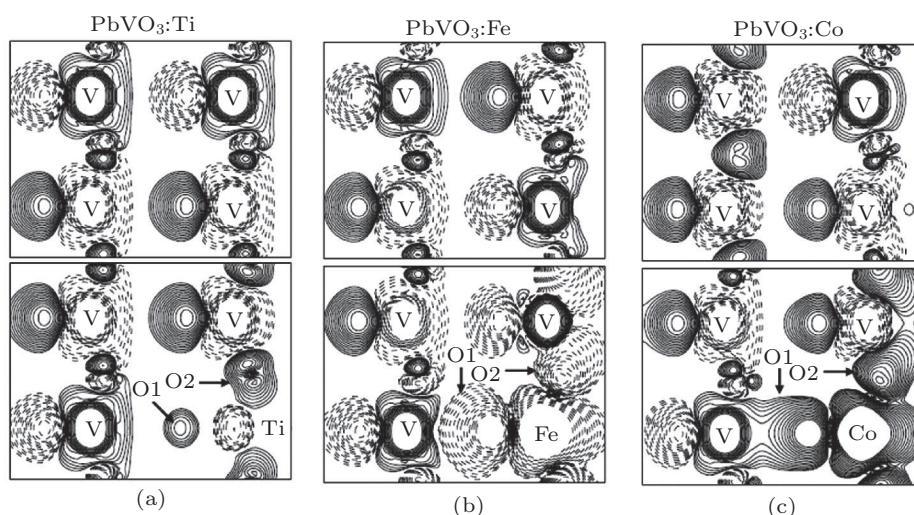


Fig. 5. The spin charge densities of $PbVO_3$ in the (010) plane across the V ions and the impurity ions of (a) Ti, (b) Fe, and (c) Co, respectively. The spin-up and spin-down densities are denoted by the solid and dashed lines, respectively. Here, the spin density contours start at $0.001 e/\text{Å}^3$ and increase successively by a factor of $\sqrt{2}$.

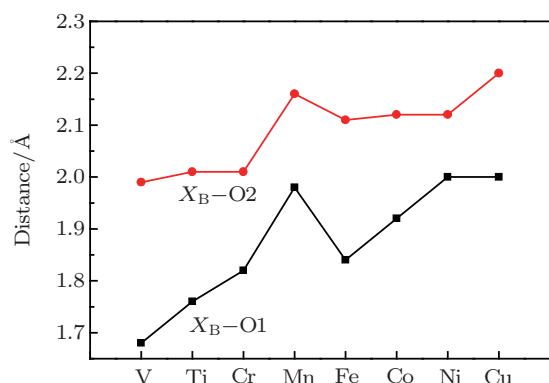


Fig. 6. (color online) The bond lengths between the B-site dopants ($X_B = V, Ti, Cr, Mn, Fe, Co, Ni,$ and Cu) and nearby O1 and O2 ions.

The large local magnetic moments of B ($X_B = Mn, Co,$ and Ni) may also have played a critical role in destabilizing the original two-dimensional AFM ordering of $PbVO_3$. The collective magnetic moments can be introduced by the various 3d transition metal doping at the B site, which is different from the scenario in the A-site-doped systems. The total mag-

netic moments among various 3d transition metal-doped systems are shown in Fig. 4. The GGA- and GGA + U -calculated total magnetic moments are clearly different in some doped systems. For example, the total magnetic moments of Cr, Fe, and Cu doped in $PbVO_3$ systems decrease when the Hubbard U correction is applied to the 3d transition metals. The total magnetic moments of the Co-doped $PbVO_3$ system increases with GGA + U calculations, while Ti-, Mn-, and Ni-doped $PbVO_3$ systems keep almost the same total magnetic moment. As a result, B-site doping in $PbVO_3$ not only removes the degenerations of C- and G-AFM spin glass, but also destabilizes the original two-dimensional AFM coupling in the a - b plane, potentially introducing remnant magnetic moments to $PbVO_3$ for magnetoelectronic applications.

The ferroelectric materials with large energy band gaps are expected to have less electrical leakage in the ferroelectric switching process. The energy band gaps of $PbVO_3$ doped by 3d transition metals are calculated by GGA + U to compare the insulating behavior with the results listed in Table 2.

Table 2. The calculated energy band gap values, and the polarization value along the $\langle 001 \rangle$ direction for $PbVO_3$ doped by the 3d transition metal.

	Pure	Ti	Cr	Mn	Fe	Co	Ni	Cu
Band gap/eV	1.80	1.59	1.61	1.60	1.38	1.81	1.13	1.12
$P_3/(\mu C/cm^2)$	156.4	147.8	151.4	155.7	147.4	158.1	132.4	143.3

The calculated value of the energy gap of pure PbVO_3 is about 1.80 eV, while it is reduced in most 3d transition metal-doped systems. In particular, the band gap of PbVO_3 reduces to about 1.30 eV when doped by Ni or Cu since they each have a higher electronegativity than the early transition metals and thus less ionic bonding with nearby O ions. The Berry phase method-calculated ferroelectric polarization values of the pure and doped system along the (001) direction are listed in Table 2, and the corresponding charge transfers based on Bader charge analysis are shown in Fig. 7.

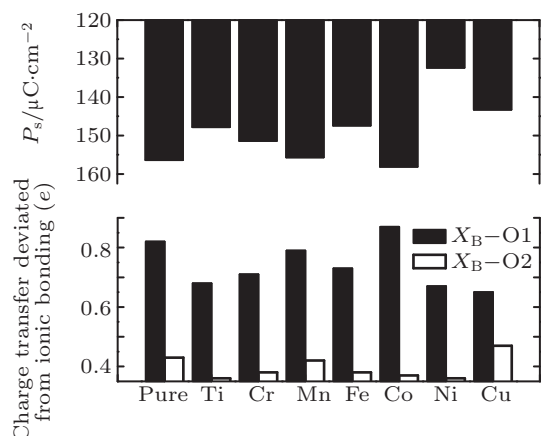


Fig. 7. The calculated charge transfer deviation from pure ionic bonding (i.e., the corresponding expected oxidation state) between the B-site doping 3d transition metals and O ions, with a corresponding comparison of the calculated ferroelectric polarization.

We find that the ferroelectric polarizations of the doped systems are correlated to the degree of ionic bonding between the B-site-doped cations and O ions, which could be indicated by the charge transfer between them. The Bader charge-calculated charge state of the Pb ion is about 1.97+ in the pure PbVO_3 and changes little in all the studied B-site-doping systems, showing its good ionic bonding properties with neighboring ions. The calculated charge state of the V ion is about 2.26+, which deviates from its expected oxidation state 4+, while the O1 and O2 valence states are 1.18– and 1.57–, indicating that the B-site ions share covalent bonding partly with nearby O ions. Typically, the charge transfers deviating from pure ionic bonding (i.e., the expected oxidation state) are $0.82e$, $0.43e$ in pure PbVO_3 between V–O1 and V–O2, while those between Co–O and Co–O2 increase to $0.87e$, $0.37e$. This leads to the fact that Co-doped PbVO_3 maintains a large ferroelectric polarization value about $158 \mu\text{C}/\text{cm}^2$. By contrast, doping Ni and Cu produces a lower charge transfer between the O ions and could decrease the ferroelectric polarizations of the systems. The long bond lengths of Ni–O and Cu–O (Fig. 6) in the doped system may also play a role in degrading the ferroelectric polarization.

6. Conclusions

In this paper, we theoretically show that a large ferroelectric polarization and a long magnetic order, even macro ferri/ferromagnetism, could be introduced by A- or B-site doping in PbVO_3 . Here, $\text{Pb}_7X_A\text{V}_8\text{O}_{24}$ ($X_A = \text{Ca}, \text{Sr}, \text{and Ba}$) are inclined to preserve the spin glass and large ferroelectric polarization. In particular, substituting Pb with La and Bi in PbVO_3 removes the spin glass effectively but destroys the ferroelectric properties, since they introduce an inner physical strain with their mismatched ion radii and turn the system into a metal. Furthermore, remnant magnetic moments can be induced by 3d transition element doping at the B site of PbVO_3 . The degenerated G- and C-AFM configurations can be clearly removed by B-site doping of Fe or Cr ions. When Mn, Co, Ni, or Cu is doped at the B site of PbVO_3 , its two-dimensional AFM coupling can also be destabilized as the spin orientations of some V ions are flipped. Most B-site 3d transition element-doped PbVO_3 can preserve its large band gap and large ferroelectric polarization, except for Ni and Cu.

Acknowledgment

We are grateful for the use of the computers at the High Performance Computer Center of the Shenzhen Institute of Advanced Technology (SIAT), Chinese Academy of Sciences, and the National Supercomputing Center in Shenzhen.

References

- [1] Schmid H 1994 *Ferroelectrics* **162** 317
- [2] Hill N A 2000 *J. Phys. Chem. B* **104** 6694
- [3] Ramesh R and Spaldin N A 2007 *Nat. Mater.* **6** 21
- [4] Shpanchenko R V, Chernaya V V, Tsirlin A A, Chizhov P S, Sklovsky D E, Antipov E V, Khlybov E P, Pomjakushin V, Balagurov A M, Medvedeva J E, Kaul E E and Geibel C 2004 *Chem. Mater.* **16** 3267
- [5] Belik A A, Azuma M, Saito T, Shimakawa Y and Takano M 2005 *Chem. Mater.* **17** 269
- [6] Singh D J 2006 *Phys. Rev. B* **73** 094102
- [7] Martin L W, Zhan Q, Suzuki Y, Ramesh R, Chi M F, Browning N, Mizoguchi T and Kreisel J 2007 *Appl. Phys. Lett.* **90** 062903
- [8] Oka K, Yamada I, Azuma M, Takeshita S, Satoh K H, Koda A, Kadono R, Takano M and Shimakawa Y 2008 *Inorg. Chem.* **47** 7355
- [9] Kumar A, Podraza N J, Denev S, Li J, Martin L W, Chu Y H, Ramesh R, Collins R W and Gopalan V 2008 *Appl. Phys. Lett.* **92** 231915
- [10] Uratani Y, Shishidou T, Ishii F and Oguchi T 2005 *Jpn. J. Appl. Phys.* **44** 7130
- [11] Kumar A, Martin L W, Denev S, Kortright J B, Suzuki Y, Ramesh R and Gopalan V 2007 *Phys. Rev. B* **75** 060101
- [12] Tsirlin A A, Belik A A, Shpanchenko R V, Antipov E V, Takayama-Muromachi E and Rosner H 2008 *Phys. Rev. B* **77** 092402
- [13] Uratani Y, Shishidou T and Oguchi T 2009 *J. Phys. Soc. Jpn.* **78** 084709
- [14] Ju S and Cai T Y 2008 *Appl. Phys. Lett.* **93** 251904
- [15] Lawes G and Srinivasan G 2011 *J. Phys. D: Appl. Phys.* **44** 243001
- [16] Solovyev IV 2012 *Phys. Rev. B* **85** 054420
- [17] Sosnowska I, Neumaier T P and Steichele E 1982 *J. Phys. C* **15** 4835
- [18] Bai F M, Wang J L, Wuttig M, Li J F, Wang N G, Pyatakov A P, Zvezdin A K, Cross L E and Viehland D 2005 *Appl. Phys. Lett.* **86** 32511
- [19] Picozzi S and Ederer C 2009 *J. Phys.: Condens. Matter* **21** 303201
- [20] Baettig P, Ederer C and Spaldin N A 2005 *Phys. Rev. B* **72** 214105
- [21] Nechache R, Harnagea C, Pignolet A, Normandin F, Veres T, Carignan L P and Menard D 2006 *Appl. Phys. Lett.* **89** 102902

- [22] Khomchenko V A, Kopcewicz M, Lopes A M L, Pogorelov Y G, Araujo J P, Vieira J M and Kholkin A L 2008 *J. Phys: D: Appl. Phys.* **41** 102003
- [23] Chang H and Zhao Y G 2011 *Chin. Phys. Lett.* **28** 067503
- [24] Ma Z Z, Li J Q, Tian Z M, Qiu Y and Yuan S L 2012 *Chin. Phys. B* **21** 107503
- [25] Khomchenko V A, Kiselev D A, Vieira J M, Jian L, Kholkin A L, Lopes A M L, Pogorelov Y G, Araujo J P and Maglione M 2008 *J. Appl. Phys.* **103** 024105
- [26] Wang D H, Goh W C, Ning M and Ong C K 2006 *Appl. Phys. Lett.* **88** 212907
- [27] Zhang S T, Zhang Y, Lu M H, Du C L, Chen Y F, Liu Z G, Zhu Y Y, Ming N B and Pan X Q 2006 *Appl. Phys. Lett.* **88** 162901
- [28] Chen X Y, Tian R Y, Wu J M, Zhao Y J, Ding H C and Duan C G 2011 *J. Phys: Condens. Matter* **23** 326005
- [29] Kresse G and Furthmuller J 1996 *Comput. Mater. Sci.* **6** 15
- [30] Kresse G and Joubert D 1999 *Phys. Rev. B* **59** 1758
- [31] Perdew J P and Wang Y 1992 *Phys. Rev. B* **45** 13244
- [32] Liechtenstein A I, Anisimov V I and Zaanen J 1995 *Phys. Rev. B* **52** R5467
- [33] Ederer C and Spaldin N A 2006 *Phys. Rev. B* **74** 024102
- [34] Ederer C, Harris T and Kovacik R 2011 *Phys. Rev. B* **83** 054110
- [35] Kingsmith R D and Vanderbilt D 1993 *Phys. Rev. B* **47** 1651
- [36] Dean J A 1979 *Lange's Handbook of Chemistry*, 12th edn. (New York: McGraw-Hill) pp. 3–124
- [37] Hafner J 2008 *J. Comput. Chem.* **29** 2044
- [38] Anderson P W 1959 *Phys. Rev.* **115** 2
- [39] Tsuchiya T, Katsumata T, Ohba T and Inaguma Y 2009 *J. Ceram. Soc. Jpn.* **117** 102